actuators

MDPI

Article

XCoM-Based Moving-Mass Control in a Backpack for Modulating Gait Stability During Load Carriage

Jangwon Lee [1] and Ho Seon Choi [2,*]

[1] Department of Intelligent Mechatronics Engineering, Sejong University, Seoul 05006, Republic of Korea; jang9379@sju.ac.kr
[2] Department of Artificial Intelligence and Robotics, Sejong University, Seoul 05006, Republic of Korea
* Correspondence: choihoseon@sejong.ac.kr

Abstract

Backpack load carriage can alter gait mechanics and dynamic stability, while existing assistive backpacks have primarily targeted load transmission and metabolic cost. This study investigated whether active vertical repositioning of a moving mass within a backpack could influence gait-stability-related outcomes. A frontal-plane double inverted pendulum model was combined with inertial measurement unit (IMU)-derived motion states to calculate a model-estimated mediolateral extrapolated center of mass (XCoM), and model predictive control (MPC) regulated a 5 kg moving mass in real time. Six participants walked on a treadmill at 1.2 m/s under a Normal condition, three fixed-mass conditions (Low, Mid, and High), and a Powered condition with XCoM-based moving-mass control. Short-term largest Lyapunov exponent (LLE), kinematic variability (KV), and trunk sway were evaluated as gait-stability-related outcomes. In the Powered condition, short-term LLE was 19.0%, 15.7%, and 24.4% lower than in the Low, Mid, and High conditions, respectively, with all six participants showing lower LLE in each comparison. However, no pairwise comparison of LLE, KV, or trunk sway remained statistically significant after Bonferroni correction. The model-estimated XCoM and filtered moving-mass velocity command were negatively correlated ($r = -0.3310$). These findings support the feasibility of state-dependent moving-mass control during load carriage and indicate the need for further evaluation of its effects on gait stability in a larger cohort.

Keywords: load carriage; model predictive control; gait stability

1. Introduction

Backpacks are among the most widely used load-carriage systems for transporting loads in military, occupational, and recreational settings. However, backpack load carriage can alter ground reaction forces, lower-limb joint kinematics, and gait patterns [1], while both load magnitude and vertical position can affect trunk posture and metabolic cost [2]. Accordingly, various assistive strategies have been investigated to reduce the burdens associated with load carriage.

Existing assistive backpack systems have primarily been developed to reduce the mechanical loads transmitted to the body and the metabolic cost of load carriage. Park et al. distributed backpack loads between the shoulders and pelvis and actively attenuated the vertical dynamic loads generated during walking, thereby reducing muscle activation, ground reaction forces, and metabolic cost [3]. Suspended-load backpacks allow the carried load to move vertically relative to the torso, thereby reducing the dynamic loads

Check for updates

Academic Editor: Ching-yi Wu

Received: 18 September 2026
Revised: 13 October 2026
Accepted: 14 October 2026
Published: 16 October 2026

Copyright: © 2026 by the authors. Licensee MDPI, Basel, Switzerland. This article is an open access article distributed under the terms and conditions of the Creative Commons Attribution (CC BY) license.

transmitted to the body [4,5], and this relative motion of the load has also been shown to reduce mechanical work and metabolic cost [6]. However, these systems have primarily focused on reducing load transmission and energy expenditure.

The magnitude and vertical position of a backpack load can alter spatiotemporal gait parameters and trunk posture [7], and load magnitude has also been reported to affect local dynamic stability [8]. Therefore, load-carriage assistance should consider not only physical and physiological demands but also dynamic gait stability. However, relatively few studies have directly addressed changes in gait stability induced by load carriage, highlighting the need for assistive strategies that adapt to changes in balance state during walking.

Lower-limb joint kinematics and kinetics have been used for gait-pattern recognition [9]. For dynamic balance, human walking relies strongly on active mediolateral balance control [10] and has been reported to be more sensitive to visual perturbations in the mediolateral direction than in the anteroposterior direction [11]. Hof et al. introduced the extrapolated center of mass (XCoM), which incorporates the position and velocity of the center of mass (CoM) to formulate conditions for dynamic stability [12]. Hof subsequently used the XCoM to describe the conditions required for stable walking [13]. Accordingly, the mediolateral XCoM may serve as a control metric for assessing changes in lateral balance during load carriage and guiding active assistance. Previous work has shown that vertical redistribution of the CoM affects postural sway during quiet standing, including its mediolateral component [14]. These findings suggest that adjusting the vertical position of a moving mass within a backpack may influence mediolateral balance by altering the mass distribution and dynamic properties of the coupled human–load system.

In this study, we propose a moving-mass backpack system that actively repositions an internal mass in the vertical direction according to the walking state. IMU-derived frontal-plane motion states were incorporated into a double inverted pendulum model to calculate a model-estimated mediolateral XCoM, which was used as the primary controlled output. A linearized dynamic model was then used within a model predictive control (MPC) framework to predict the future evolution of the model-estimated XCoM and determine the moving-mass velocity command in real time to reduce the predicted XCoM deviation from the reference. Gait experiments were conducted to quantify the magnitude of the model-estimated XCoM, examine its relationship with the filtered moving-mass velocity command, and evaluate gait-stability-related outcomes, thereby assessing active moving-mass repositioning as a strategy for modulating gait-stability-related dynamics during load carriage.

2. Materials and Methods

2.1. Human–Moving-Mass Modeling

To simplify the mediolateral dynamics of the human–moving-mass system during walking, the human body was represented as a frontal-plane double inverted pendulum consisting of a lower-limb link and a trunk link, as illustrated in Figure 1a. The lower-limb link was modeled as a rigid body rotating about the ankle joint, and the trunk link was modeled as a rigid body rotating about the hip joint, thereby accounting for the contributions of lower-limb and trunk motions to mediolateral CoM displacement. The moving mass was modeled as an external mass translating along a prismatic joint mounted posterior to the trunk, with the translation axis defined relative to a coordinate frame fixed to the trunk link. Based on this model structure, the physical parameters of the human segments and moving mass were defined.

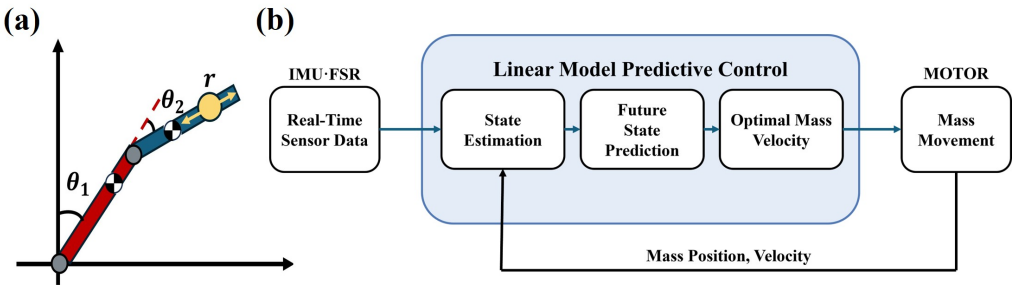


Figure 1. Overview of the modeling and control framework for the proposed moving-mass backpack system. (**a**) Frontal-plane double inverted pendulum model of the human–moving-mass system; (**b**) real-time model predictive control (MPC) framework based on the extrapolated center of mass (XCoM).

The anthropometric parameters of the human segments were defined based on the dimensions of a young adult male with a body mass of 84.14 kg and a height of 1.79 m [15]. These reference anthropometric parameters were used for all participants during the walking experiments. The masses, lengths, center-of-mass locations, and moments of inertia of the lower-limb and trunk links were determined from the anthropometric parameters, whereas the mass and travel range of the moving mass were defined according to the mechanical specifications of the fabricated device. The principal model parameters used in this study are listed in Table 1 and were used to define the generalized coordinates and system dynamics.

Table 1. Model parameters used in the human–moving-mass model.

Symbol	Description	Value
m_1	Mass of the lower-limb link	28.047 kg
m_2	Mass of the trunk link	56.093 kg
m_3	Moving mass	5.000 kg
l_1	Length of the lower-limb link	0.900 m
l_{1c}	Distance from the ankle to the lower-limb CoM	0.576 m
l_{2c}	Distance from the hip to the trunk CoM	0.318 m
I_1	Moment of inertia of the lower-limb link	9.305 kg·m^2
I_2	Moment of inertia of the trunk link	5.674 kg·m^2
r	Moving-mass position	0–0.400 m

The generalized coordinates of the human model were defined as

$$\mathbf{q} = \begin{bmatrix} \theta_1 & \theta_2 \end{bmatrix}^T, \tag{1}$$

where θ_1 denotes the absolute angle of the lower-limb link with respect to the vertical axis, and θ_2 denotes the angle of the trunk link relative to the lower-limb link. The moving-mass position, $r(t)$, was defined separately from the generalized coordinates. The equations of motion were then derived by applying Lagrange's equations to the system dynamics, including the moving mass:

$$\mathbf{M}(\mathbf{q}, r)\ddot{\mathbf{q}} + \mathbf{C}(\mathbf{q}, \dot{\mathbf{q}}, r, \dot{r}) + \mathbf{G}(\mathbf{q}, r) = \mathbf{0}, \tag{2}$$

where $\mathbf{M}$ denotes the inertia matrix, $\mathbf{C}$ represents the nonlinear terms associated with joint and moving-mass motion, and $\mathbf{G}$ represents the gravitational terms. For the simplified prediction model used in the MPC, active joint torques generated at the ankle and hip were not explicitly modeled, and the corresponding generalized forces were assumed to be zero. This simplification was adopted to enable real-time MPC implementation on the embedded

controller. Although active joint torques were omitted from the prediction model, the controller state was re-estimated from IMU measurements at each control step, such that the measured kinematic consequences of human joint actions were incorporated into the current-state update. However, the effects of active joint torques on future state evolution over the prediction horizon were not explicitly predicted. The actuation force of the moving mass was also not explicitly modeled; instead, the moving-mass velocity command was subsequently treated as the control input to the MPC.

2.2. XCoM-Based Linear MPC

A linear MPC was implemented to regulate the moving mass in real time according to the time-varying controller state during walking. Figure 1b illustrates the overall real-time control framework, in which the controller state was estimated from sensor measurements, future states were predicted by the MPC, and the optimal moving-mass velocity sequence was computed to actuate the moving mass. Based on the human–moving-mass dynamics derived in Section 2.1, the controller predicted the future controller states over the prediction horizon and determined the moving-mass velocity command by minimizing the predicted model-estimated XCoM deviation while satisfying the moving-mass constraints. Constraints on the moving-mass position and velocity were imposed to ensure that the controller operated within the allowable mechanical limits.

2.2.1. XCoM Estimation

The mediolateral XCoM was defined as the primary controlled output of the MPC. First, using the double inverted pendulum model defined in Section 2.1, the mediolateral position of the human CoM was approximated as a linear function of the generalized angular coordinates:

$$x_{\mathrm{CoM}} = a_1\theta_1 + a_2\theta_2, \tag{3}$$

where a_1 and a_2 are coefficients that relate lower-limb and trunk rotations to mediolateral CoM displacement and are determined by the mass distribution and geometric parameters of the human segments.

The XCoM was calculated from the position and velocity of the CoM as

$$XCoM = x_{\mathrm{CoM}} + \frac{\dot{x}_{\mathrm{CoM}}}{\sqrt{\frac{g}{h_{\mathrm{CoM}}}}}, \tag{4}$$

where g is the gravitational acceleration and h_{CoM} is the human CoM height in the reference posture, defined as

$$h_{\mathrm{CoM}} = \frac{m_1 l_{1c} + m_2(l_1 + l_{2c})}{m_1 + m_2}. \tag{5}$$

To retain the linear inverted pendulum approximation underlying the XCoM formulation, h_{CoM} was treated as a constant evaluated at the reference posture. Accordingly, the XCoM was expressed as a linear function of the angular states defined in the model. The moving-mass position r was not directly included in the XCoM calculation; rather, it was incorporated as a state variable in the dynamic model of the human–moving-mass system. In the real-time implementation, IMU-derived frontal-plane ankle and hip motion states were used to form the angular components of the controller state vector. The XCoM calculated from these controller states is hereafter referred to as the model-estimated XCoM.

2.2.2. Linear Predictive Model

To incorporate the XCoM defined above as a predicted output of the MPC, the human–moving-mass system was formulated as a linear state-space model. The state vector was defined as

$$\mathbf{x}(k) = \begin{bmatrix} \theta_1(k) & \dot{\theta}_1(k) & \theta_2(k) & \dot{\theta}_2(k) & r(k) \end{bmatrix}^T, \tag{6}$$

and the control input was defined as

$$u(k) = \dot{r}_{\mathrm{cmd}}(k). \tag{7}$$

By incorporating the relationship between the moving-mass position and its velocity command, the nonlinear dynamics described in Section 2.1 were linearized about the reference posture and discretized, yielding the following state-space representation:

$$\mathbf{x}(k+1) = \mathbf{A}\mathbf{x}(k) + \mathbf{B}u(k), \tag{8}$$

$$\mathbf{y}(k) = \begin{bmatrix} XCoM(k) \\ r(k) \end{bmatrix} = \mathbf{N}\mathbf{x}(k). \tag{9}$$

The output vector $\mathbf{y}(k)$ consisted of the model-estimated XCoM and moving-mass position. The model-estimated XCoM served as the primary controlled output, while the moving-mass position was included to penalize deviations from its reference position and to impose constraints on the allowable travel range.

At each control step, the MPC predicted the system outputs over the prediction horizon based on the current state and a sequence of future control inputs. Following the matrix-based predictive formulation for embedded MPC implementation [16], the state-space model was extended over the prediction horizon, yielding the following relationship between the predicted outputs and control inputs:

$$\mathbf{Y} = \bar{\mathbf{M}}\mathbf{x}(k) + \bar{\mathbf{L}}\mathbf{U}, \tag{10}$$

where $\mathbf{Y}$ is the stacked output vector over the prediction horizon, $\mathbf{U}$ is the stacked control-input vector, and $\bar{\mathbf{M}}$ and $\bar{\mathbf{L}}$ are the prediction matrices constructed from the state-space model. Thus, the predicted outputs were expressed as a linear function of the current state and future control inputs.

2.2.3. MPC Objective Function

The MPC objective function was formulated to minimize the tracking errors of the model-estimated XCoM and moving-mass position relative to their respective reference values over the prediction horizon while penalizing excessive moving-mass velocity commands. The cost function for the output tracking error and control input was defined as

$$J = (\mathbf{Y} - \mathbf{Y}_{\mathrm{ref}})^T \mathbf{Q} (\mathbf{Y} - \mathbf{Y}_{\mathrm{ref}}) + \mathbf{U}^T \mathbf{R} \mathbf{U}. \tag{11}$$

The reference output vector, $\mathbf{Y}_{\mathrm{ref}}$, consisted of the desired model-estimated XCoM and moving-mass position. The model-estimated XCoM reference was set to zero, corresponding to the neutral position of the reference posture in the frontal plane, and the reference position of the moving mass was set to the midpoint of its allowable travel range. $\mathbf{Q}$ is the weighting matrix associated with the tracking errors of the two outputs, and $\mathbf{R}$ is the weighting matrix associated with the moving-mass velocity command.

The MPC parameters were empirically tuned through preliminary tests conducted prior to the walking experiments. The output weights were selected to place greater

emphasis on model-estimated XCoM regulation than on maintaining the moving mass near its reference position, while the input weight was selected to penalize excessive moving-mass velocity commands. The final MPC parameters and constraints are summarized in Table 2.

Table 2. Parameters and constraints used in the MPC implementation.

Parameter	Symbol	Value
Prediction horizon	N_p	20
Control horizon	N_c	5
XCoM tracking weight	Q_{XCoM}	1000
Moving-mass position weight	Q_r	10
Control-input weight	R	1×10^{-3}
Moving-mass position constraint	r	$[0,\ 0.400]$ m
Moving-mass velocity constraint	$\dot{r}_{\mathrm{cmd}}$	$[-0.25,\ 0.25]$ m/s

Substituting the predicted output in Equation (10) into the cost function in Equation (11) yields a quadratic function of the control-input sequence $\mathbf{U}$. The resulting optimization problem can therefore be formulated as the following quadratic programming (QP) problem:

$$\min_{\mathbf{U}} \mathbf{U}^T \mathbf{H} \mathbf{U} + \mathbf{g}_{\mathrm{QP}}^T \mathbf{U}, \tag{12}$$

where $\mathbf{H}$ is the Hessian matrix associated with the quadratic term of the objective function, and $\mathbf{g}_{\mathrm{QP}}$ is the linear-term vector determined by the current state and reference output. The QP problem was solved in real time using qpOASES [17], with constraints imposed on the moving-mass position and velocity. At each control step, the optimal sequence of velocity commands was computed, and only the first control input was applied to the moving-mass actuator in a receding-horizon manner. This procedure enabled the moving mass to be regulated to reduce model-estimated XCoM deviations while satisfying the mechanical constraints of the device.

2.3. System Design

The proposed system comprised a mechanical structure, an actuation and control system, and a sensing system for measuring human motion, enabling active adjustment of a moving mass located posterior to the torso according to the walking state represented by the model-estimated XCoM.

2.3.1. Mechanical Design

Figure 2 illustrates the mechanical structure and actuation principle of the proposed moving-mass backpack system. The device consisted of a structural frame and a cable-driven actuation mechanism comprising two motors (DM-J4310-2EC, Shenzhen, China), motor pulleys, cables, linear guides, sliders, and a load frame. The cables were anchored at the upper and lower ends of the backpack frame, while the motor-pulley units were mounted on opposite sides of the load frame. Rotation of the motor pulleys wound or unwound the cables, thereby translating the load frame vertically along the guide rails. The two motors were operated simultaneously to provide symmetric actuation and reduce tilting of the load frame during vertical translation.

The linear guides were rigidly attached to the upper and lower aluminum profiles using mounting components. The mounting components connecting the aluminum profiles and linear guides, the pulleys, and selected components of the load frame were fabricated from polylactic acid (PLA) using 3D printing. The entire frame was securely attached to the wearer's torso using shoulder, waist, and chest straps to maintain stable positioning

during walking. The backpack system weighed 3.2 kg, excluding the actively driven 5 kg moving mass.

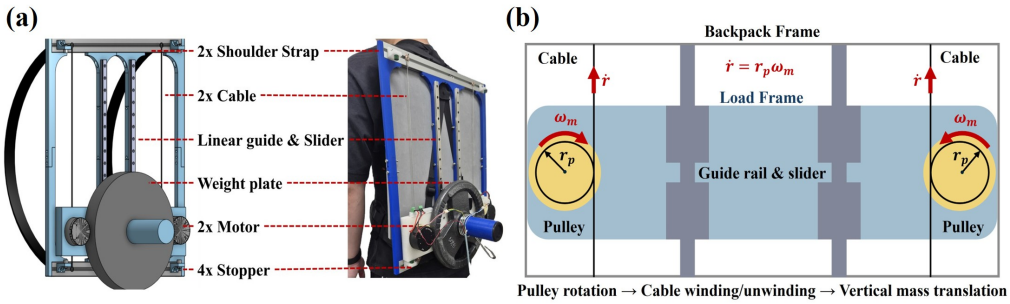


Figure 2. Mechanical configuration and actuation principle of the moving-mass backpack. (**a**) Main components and assembled configuration of the backpack system. (**b**) Cable-driven vertical actuation mechanism. Rotation of the motor pulleys winds or unwinds the cables, translating the load frame along the guide rails. Here, ω_m, r_p, and $\dot{r}$ denote the motor angular velocity, pulley radius, and moving-mass velocity, respectively, with $\dot{r} = r_p\omega_m$ under the motor-direction convention used in the controller.

2.3.2. Electrical and Embedded System

The real-time control system consisted of IMUs (EBIMU24GV6, E2BOX, Hanam-si, Republic of Korea), force-sensitive resistors (FSRs), two motors for actuating the moving mass, and an STM32F407G-DISC1 microcontroller.

IMU and FSR signals were acquired in real time at 1000 Hz. Foot-contact information from the FSRs was used to identify the stance side for real-time control. For the selected stance side, the IMU-derived frontal-plane ankle motion states were assigned to the controller-state components θ_1 and $\dot{\theta}_1$, while the corresponding hip motion states were assigned to θ_2 and $\dot{\theta}_2$. Together with the moving-mass position r, these states were supplied to the MPC. The MPC solved the optimization problem at 200 Hz to generate the moving-mass velocity command. The QP computation time was 1.130 ± 0.105 ms, with a maximum of 2.070 ms, remaining within the 5-ms control interval. The 95th-percentile changes in θ_1 and θ_2 over the QP computation interval were approximately 0.21° and 0.27°, respectively. The command was passed through a low-pass filter with a cutoff frequency of 3 Hz before being transmitted to the motors. The cutoff frequency was empirically selected through preliminary tests to reduce high-frequency command fluctuations while preserving responsiveness to changes in gait state. The 3-Hz low-pass filter introduced a calculated phase delay of approximately 51 ms at 1 Hz.

2.4. Experimental Setup

2.4.1. Participants

Six participants (height: 1.72 ± 0.07 m; body mass: 68.2 ± 7.3 kg; age: 27 ± 1 years) participated in the experiment. All experimental procedures were approved by the Institutional Review Board of Sejong University (SUIRB-HR-2026-024). The experimental procedures and study protocol were explained to all participants both verbally and in writing before participation. Participants were recruited through a recruitment notice, and the eligibility criteria required them to be healthy with no self-reported history of gait abnormalities or related disorders. Written informed consent was obtained from all participants prior to the experiment. The experimental setup and operation of the proposed system are shown in Video S1.

2.4.2. Experimental Protocol

The experiment consisted of five conditions: Normal, in which participants walked without wearing the device; Low, Mid, and High, in which the moving mass was fixed at 0, 0.200, and 0.400 m along the linear guide, respectively; and Powered, in which the moving mass was actively controlled using XCoM-based MPC (Figure 3). Under all conditions, participants walked with their arms crossed over their chest to minimize balance compensation through arm movements.

Participants walked on a treadmill at a speed of 1.2 m/s under each condition, and IMU, FSR, moving-mass position, and control data were simultaneously recorded. The order of the experimental conditions was varied across participants to minimize order effects, and sufficient rest was provided between trials to reduce the potential effects of fatigue. The first 1 min of each trial was excluded from the analysis. The subsequent 3 min of walking data were used for analysis.

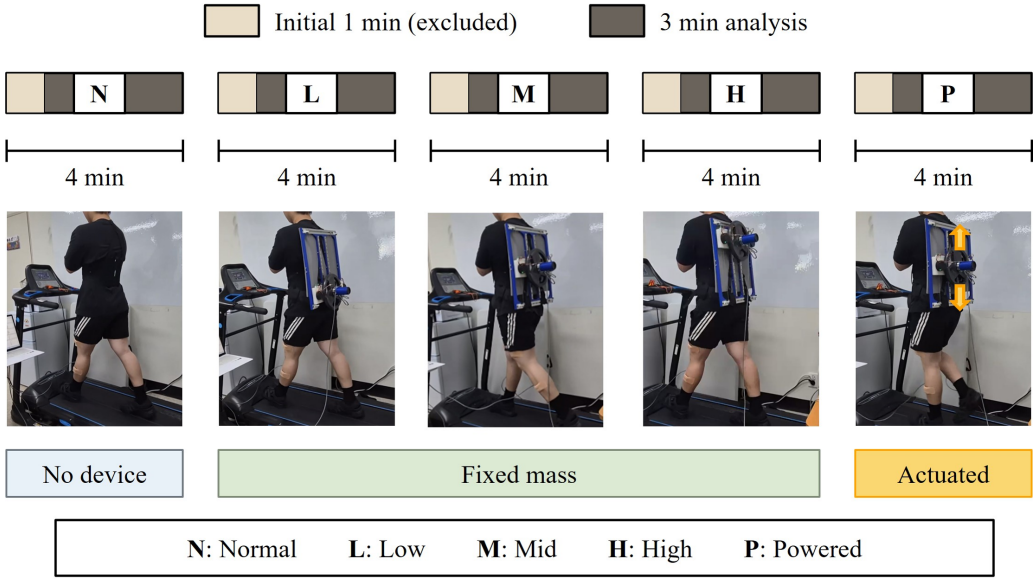


Figure 3. Experimental conditions and protocol. Participants performed treadmill walking under the Normal, Low, Mid, High, and Powered conditions. The first 1 min of each trial was excluded from the analysis, and the subsequent 3 min of walking data were used for analysis. The actual condition order was varied across participants.

2.5. Data Processing

Gait cycles were segmented based on heel strikes detected from the left-foot FSR signal. A heel strike was defined as the instant at which the FSR signal exceeded a predefined threshold, and the interval between two consecutive heel strikes of the same foot was defined as one gait cycle.

IMU data were used to estimate the orientations of the lower-limb and trunk segments during walking. A total of eight IMUs were used: six were attached bilaterally to the thighs, shanks, and feet, and one IMU each was attached to the pelvis and trunk. Prior to the experiment, gravity vectors measured in two calibration postures were used to define and normalize the sensor axes, thereby aligning each sensor coordinate system with the corresponding body-segment coordinate system. Segment orientations were subsequently estimated during walking, and frontal-plane ankle and hip motion states were obtained from adjacent body segments [18]. These IMU-derived motion states were used as the angular components of the controller state vector.

The model-estimated XCoM was calculated from the IMU-derived motion states using the formulation described in Section 2.2.1. Each gait cycle was time-normalized from 0% to 100% and interpolated to 101 points.

2.6. Measurements

The model-estimated XCoM RMS and participant-specific and pooled Pearson correlations between the model-estimated XCoM and the filtered moving-mass velocity command were evaluated separately from the gait-stability-related outcomes, which comprised local dynamic stability, kinematic variability, and trunk sway.

Local dynamic stability was quantified using the short-term largest Lyapunov exponent (LLE) derived from trunk IMU signals. Local dynamic stability reflects the sensitivity of the locomotor system to small perturbations and has been widely used to assess gait stability [19]. A state space was constructed from the time-normalized triaxial trunk acceleration signals, and the mean logarithmic divergence curve between neighboring trajectories was calculated. A least-squares linear fit was applied over the 0–0.5 stride interval, and the slope of the fitted line was defined as the short-term LLE. A larger LLE indicates more rapid divergence of neighboring trajectories and, consequently, lower local dynamic stability.

Kinematic variability (KV) was calculated to quantify the variability of trunk motion across repeated gait cycles [20]. For each acceleration axis, the standard deviation (SD) across repeated gait cycles was calculated at each time point of the time-normalized gait cycle and then averaged over the entire gait cycle. The resulting values from the three axes were subsequently combined using the RMS to obtain a single KV value. A larger KV indicates greater variability and lower consistency of movement patterns across repeated gait cycles.

Trunk sway was calculated from the two trunk acceleration components orthogonal to the gravity-aligned vertical axis to quantify the magnitude of trunk motion during walking. For each condition, the two acceleration components obtained across gait cycles were represented in a two-dimensional space, and a Gaussian ellipse was constructed from their covariance matrix. The standard deviations along the two principal axes of the ellipse were determined from the eigenvalues of the covariance matrix, and the RMS of these two standard deviations was defined as the trunk sway for that condition. A larger value indicates greater trunk motion during walking.

The model-estimated XCoM RMS was calculated across all conditions to compare the overall magnitude of the model-estimated XCoM between the fixed-mass and Powered conditions. For each condition, the RMS was calculated from the model-estimated XCoM samples within the analyzed gait cycles. A larger value indicates a greater overall magnitude of the model-estimated XCoM relative to zero.

Motor velocity tracking was evaluated by comparing the filtered velocity command with the encoder-derived motor velocity. The tracking error was quantified using the root mean square error (RMSE) for each motor in the Powered condition.

To evaluate the influence of individual anthropometric parameters on MPC commands, the prediction model and QP matrices were regenerated using each participant's body mass and height. The reference and participant-specific models were evaluated using the same ankle and hip motion data and moving-mass positions recorded during the Powered condition. The MPC weights and constraints were unchanged. The first optimized velocity commands were compared using RMSE and Pearson's correlation coefficient.

2.7. Statistical Analysis

For each participant and condition, the LLE, KV, trunk sway, and model-estimated XCoM RMS were calculated using the 3-min analysis period and normalized to the corre-

sponding Normal-condition values from the same participant. The participant was treated as the statistical unit ($N = 6$). Comparisons between the Powered condition and each of the Low, Mid, and High conditions were performed using the Wilcoxon signed-rank test. A Bonferroni correction was applied to account for the three pairwise comparisons for each metric. Both unadjusted and Bonferroni-adjusted p-values are reported, with an adjusted $p < 0.05$ considered statistically significant. All statistical analyses were performed using MATLAB R2026a (MathWorks, Natick, MA, USA).

3. Results

3.1. Local Dynamic Stability

The Powered condition exhibited a numerically lower short-term LLE than all fixed-mass conditions (Figure 4a). The normalized LLE values were 0.976 ± 0.127 in the Low condition, 0.937 ± 0.139 in the Mid condition, 1.046 ± 0.206 in the High condition, and 0.790 ± 0.112 in the Powered condition.

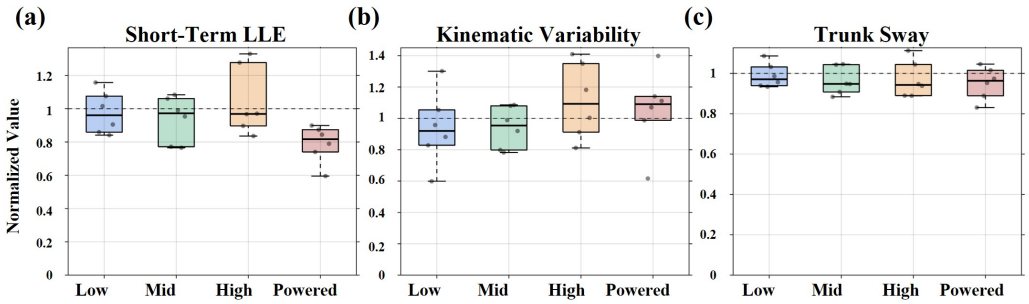


Figure 4. Normalized gait-stability-related outcomes across the fixed-mass and Powered conditions. (**a**) Short-term largest Lyapunov exponent (LLE); (**b**) kinematic variability (KV); and (**c**) trunk sway. Values were normalized to the corresponding Normal condition for the same participant, and gray dots represent individual participants. Comparisons between the Powered condition and each fixed-mass condition were performed using Wilcoxon signed-rank tests with Bonferroni correction.

The short-term LLE in the Powered condition was 19.0%, 15.7%, and 24.4% lower than the corresponding values in the Low, Mid, and High conditions, respectively. All six participants exhibited a lower LLE in the Powered condition than in each of the three fixed-mass conditions. The unadjusted p-value was 0.03125 for all three comparisons, and the corresponding Bonferroni-adjusted p-value was 0.09375. None of the differences reached statistical significance after Bonferroni correction.

3.2. Kinematic Variability

The normalized KV values were 0.937 ± 0.235 in the Low condition, 0.942 ± 0.133 in the Mid condition, 1.112 ± 0.242 in the High condition, and 1.054 ± 0.255 in the Powered condition (Figure 4b).

KV in the Powered condition was 12.5% and 11.8% higher than the corresponding values in the Low and Mid conditions, respectively, and 5.2% lower than the value in the High condition. The unadjusted and Bonferroni-adjusted p-values were 0.03125 and 0.09375 for Low, 0.15625 and 0.46875 for Mid, and 0.68750 and 1.000 for High, respectively. None of the differences reached statistical significance after Bonferroni correction.

3.3. Trunk Sway

The normalized trunk sway values were 0.989 ± 0.060 in the Low condition, 0.963 ± 0.068 in the Mid condition, 0.970 ± 0.090 in the High condition, and 0.951 ± 0.080 in the Powered condition (Figure 4c).

Trunk sway in the Powered condition was 3.8%, 1.2%, and 1.9% lower than the corresponding values in the Low, Mid, and High conditions, respectively. The unadjusted and Bonferroni-adjusted p-values were 0.15625 and 0.46875 for Low, 0.84375 and 1.000 for Mid, and 0.68750 and 1.000 for High, respectively. None of the differences reached statistical significance after Bonferroni correction.

3.4. Model-Estimated XCoM and Moving-Mass Control

Figure 5 shows representative signals over a single gait cycle in the Powered condition, illustrating the temporal profiles of the four angular controller states, moving-mass position, model-estimated XCoM, and filtered moving-mass velocity command during real-time moving-mass control.

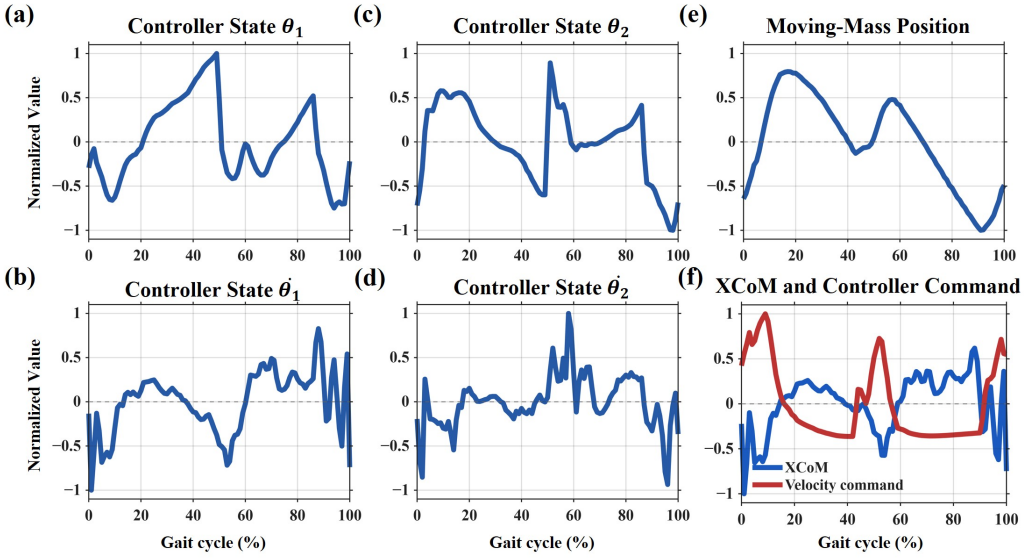


Figure 5. Representative signals over a single gait cycle in the Powered condition. (**a**) Controller state θ_1; (**b**) controller state $\dot{\theta}_1$; (**c**) controller state θ_2; (**d**) controller state $\dot{\theta}_2$; (**e**) moving-mass position; and (**f**) model-estimated XCoM and filtered moving-mass velocity command. Each signal was amplitude-normalized by subtracting its mean and dividing by its maximum absolute deviation from the mean.

The Pearson correlation coefficient between the model-estimated XCoM and the filtered moving-mass velocity command in the Powered condition was $r = -0.3310$ (Figure 6a), indicating an overall negative linear relationship between the two signals. The participant-specific Pearson correlation coefficients were −0.334, −0.528, −0.155, −0.277, −0.488, and −0.462. All six participants exhibited negative correlations, although their magnitudes varied. Across both motors and the six participants in the Powered condition, the velocity tracking RMSE ranged from 0.0091 to 0.0178 m/s.

The normalized model-estimated XCoM RMS values were 1.008 ± 0.107 in the Low condition, 1.056 ± 0.139 in the Mid condition, 1.264 ± 0.208 in the High condition, and 1.095 ± 0.099 in the Powered condition (Figure 6b). The model-estimated XCoM RMS in the Powered condition was 8.7% and 3.7% higher than the corresponding values in the Low and Mid conditions, respectively, and 13.4% lower than the value in the High condition. The unadjusted and Bonferroni-adjusted p-values were 0.06250 and 0.18750 for Low, 0.84375 and 1.000 for Mid, and 0.15625 and 0.46875 for High, respectively. None of the differences reached statistical significance after Bonferroni correction. The maximum absolute value of the model-estimated XCoM was 3.628 m. Across the six participants in the Powered condition, the RMS of the angular-velocity-related term (0.270–0.919 m) exceeded that of the position-related term (0.079–0.300 m). The angular-velocity-related term was the main contributor to the large model-estimated XCoM values.

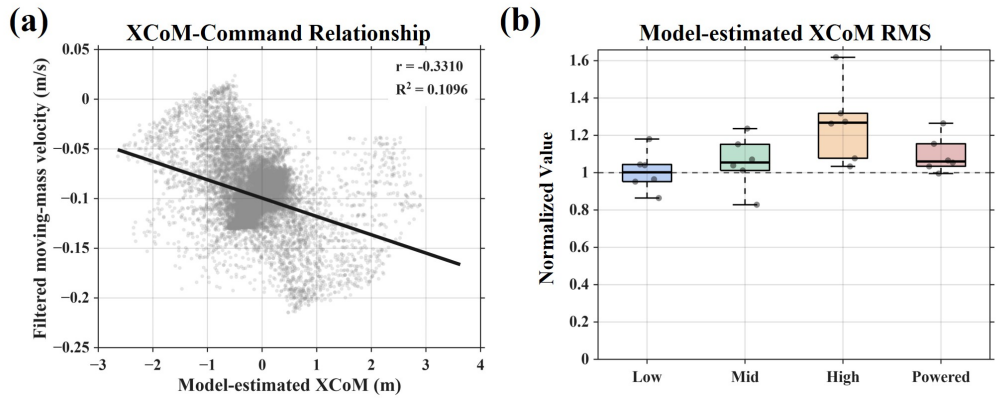


Figure 6. Model-estimated XCoM and moving-mass control results. (**a**) Relationship between the model-estimated XCoM and the filtered moving-mass velocity command in the Powered condition. The solid line represents the linear regression line. (**b**) Model-estimated XCoM RMS normalized to the corresponding Normal condition, showing the overall magnitude of the model-estimated XCoM across the fixed-mass and Powered conditions. Gray dots represent individual participants. Comparisons between the Powered condition and each fixed-mass condition were performed using Wilcoxon signed-rank tests with Bonferroni correction.

In the offline sensitivity analysis, the MPC commands calculated with participant-specific parameters differed from those obtained with the reference parameters by an RMSE of 0.0235 ± 0.0149 m/s (mean $\pm$ SD, $N = 6$). The mean Pearson correlation coefficient between the two command sequences was 0.9853 ± 0.0087.

4. Discussion

In this study, IMU-derived frontal-plane motion states were incorporated into a linear MPC framework, in which the model-estimated XCoM served as the primary controlled output for regulating the moving mass in real time. Among the gait-stability-related outcomes, short-term LLE was numerically lower in the Powered condition than in all fixed-mass conditions for all six participants, whereas KV and trunk sway showed condition-dependent changes. However, none of the pairwise differences remained statistically significant after Bonferroni correction. The model-estimated XCoM and filtered moving-mass velocity command exhibited an overall negative linear relationship. These results should therefore be interpreted as preliminary observations of the gait response to state-dependent moving-mass control rather than as evidence of an overall improvement in gait stability.

The observed negative correlation between the model-estimated XCoM and the filtered moving-mass velocity command is consistent with state-dependent modulation of the moving-mass command during walking. Although the linear relationship between the two signals was relatively weak, the MPC output was not simply proportional to the instantaneous model-estimated XCoM. Rather, the velocity command was determined by the predicted states, the current position of the moving mass, penalties on deviations from the reference position and on control effort, and constraints on the position and velocity of the moving mass. In addition, because the moving mass was actuated vertically, the controller did not directly impose a mediolateral displacement of the CoM but was intended to influence the model-estimated XCoM indirectly through changes in the dynamics of the human–moving-mass system. The limited moving-mass magnitude and displacement range, as well as the phase lag introduced by the low-pass filter applied to the moving-mass velocity command, may have constrained the response to rapid changes in gait state and reduced the linear correlation between the model-estimated XCoM and the filtered moving-

mass velocity command. However, because these factors were not evaluated independently in the present study, their individual effects cannot be distinguished.

The model-estimated XCoM RMS quantified the overall magnitude of the model-estimated XCoM relative to zero and should not be interpreted as a direct measure of dynamic stability because it does not account for the relationship between XCoM and the boundaries of the base of support (BoS) [12]. In the present study, the model-estimated XCoM RMS was numerically higher in the Powered condition than in the Low and Mid conditions and lower than in the High condition, although none of these differences remained statistically significant after Bonferroni correction. The moving-mass position was not directly included in the XCoM calculation; therefore, the observed differences in XCoM RMS reflect differences in the IMU-derived motion states used to calculate the model-estimated XCoM. Any influence of active moving-mass repositioning on the model-estimated XCoM would therefore have occurred indirectly through changes in human motion, but this mechanism was not independently evaluated in the present study. This condition-dependent result does not necessarily conflict with the MPC objective, because the controller minimized the predicted model-estimated XCoM tracking error over a finite horizon while simultaneously considering moving-mass position, control effort, and actuator constraints. Therefore, the realized model-estimated XCoM RMS was not necessarily expected to be lower than that of every fixed-mass condition. Accordingly, the observed differences in model-estimated XCoM RMS should not be interpreted as direct changes in whole-body dynamic stability.

Short-term LLE was numerically lower in the Powered condition than in all three fixed-mass conditions for all six participants. However, none of the comparisons remained statistically significant after Bonferroni correction, and the present experimental design does not establish a direct causal relationship between moving-mass repositioning and the observed LLE changes. Further experiments that independently manipulate the magnitude and timing of moving-mass motion would be required to determine this relationship.

The numerically higher KV observed in the Powered condition relative to the Low condition may be associated with adjustments in movement strategy in response to the dynamically changing assistive environment, although this difference did not remain statistically significant after Bonferroni correction. Abram et al. reported that movement variability increased upon initial exposure to a powered ankle exoskeleton and subsequently decreased with repeated experience as participants adapted to the assistive environment [21]. Similarly, in the present study, the continuously changing position of the moving mass exposed participants to a mechanical environment that differed from that of the fixed-mass conditions, and stride-to-stride adjustments to this changing environment may have contributed to the observed KV response. Although the same initial 1-min period was excluded from all conditions, no dedicated familiarization period was provided for the Powered condition. Therefore, condition-specific adaptation to the dynamically changing assistance cannot be excluded, and whether the observed KV response would decrease with longer exposure remains unknown. However, higher KV does not necessarily indicate a deterioration in local dynamic stability. KV quantifies stride-to-stride dispersion of repeated movement patterns, whereas short-term LLE quantifies the local divergence of neighboring trajectories. Dingwell and Marin demonstrated that kinematic variability can increase while local dynamic stability improves [22]. Therefore, KV and short-term LLE should be interpreted as reflecting different aspects of gait dynamics rather than as equivalent measures of stability.

The present study differs from previous backpack assistance systems by using walking-state-dependent active repositioning of the carried mass. Whereas previous systems have primarily been developed to reduce the mechanical load transmitted to the body and

the metabolic cost associated with load carriage [3–6], the present approach uses state-dependent mass repositioning to modify the dynamics of the coupled human–moving-mass system. This approach suggests that dynamic repositioning of the carried mass may provide an active strategy for modulating gait-stability-related dynamics during load carriage.

Several limitations should be considered when interpreting these findings. First, the same set of representative anthropometric parameters was applied to all participants; therefore, participant-specific differences in body-segment geometry and mass distribution were not explicitly represented and may have affected the model-estimated XCoM and corresponding MPC predictions. The offline analysis showed highly correlated MPC commands between the reference and participant-specific models, but did not evaluate the effects of participant-specific MPC during walking. Because active ankle and hip joint torques were not explicitly modeled over the MPC prediction horizon, the model did not account for their direct contribution to future state evolution, limiting the physiological fidelity of the simplified prediction model. In addition, the angular components of the controller state vector were derived from IMU-based frontal-plane ankle and hip motion rather than from direct whole-body kinematic measurements. Because these controller states were estimated from relative IMU orientations, their absolute magnitudes may have been affected by calibration offsets, sensor-to-segment alignment, and angular-velocity estimation errors. Moreover, the CoM representation and MPC prediction model were linearized about the reference posture, and their accuracy over the relatively large angular-state excursions observed in the recorded data was not independently evaluated. Therefore, the resulting model-estimated XCoM should be interpreted as a model-based controlled output rather than as a direct measurement of whole-body XCoM. The model-estimated XCoM was not validated against an independent whole-body reference; therefore, its absolute estimation error could not be quantified in the present study. These modeling and state-estimation assumptions may have introduced discrepancies between the predicted and actual human–device dynamics and thereby affected controller performance. Although the QP computation time remained within the 5-ms control interval, the complete end-to-end delay from sensor acquisition to mechanical moving-mass response was not independently measured. Motor-drive saturation was not independently quantified in the present study. The 0.4-m travel range was constrained by the physical dimensions of the backpack-type structure, thereby limiting moving-mass repositioning and the control authority of the present system.

Second, whole-body kinematics, ground reaction forces, and human–device interaction forces were not measured; therefore, the specific biomechanical mechanisms underlying the observed changes in gait-stability-related outcomes could not be determined. Electromyography (EMG) signals were also not recorded, preventing direct assessment of whether the changes in KV under the Powered condition were associated with neuromuscular adaptation. The experiments were conducted at a single walking speed with one moving-mass magnitude and controller configuration, and no dedicated familiarization period was provided for the Powered condition. Finally, the sample size was limited to six participants, which limits the statistical power and generalizability of the findings. Therefore, the present results should be interpreted as preliminary proof-of-concept findings, and further studies with larger cohorts are required to establish their reproducibility and generalizability.

Future studies should aim both to improve the performance of the moving-mass controller and to clarify the mechanisms underlying the observed changes in gait-stability-related outcomes. Quantifying and reducing signal-processing and actuation delays and systematically evaluating the effects of walking speed, moving-mass magnitude, actuation velocity, and range of motion on controller performance will be important. Participant-specific anthropometric parameterization and independent validation of the

model-estimated XCoM should also be considered to improve model fidelity and evaluate estimation accuracy. In addition, incorporating complementary stability measures, including the margin of stability, together with whole-body kinematics, ground reaction forces, human–device interaction forces, and muscle activity would enable a more detailed investigation of the biomechanical and neuromuscular mechanisms associated with the observed changes in local dynamic stability during moving-mass control. Further studies should also examine different carried loads, fatigue conditions, and overground walking to assess the practical applicability of the system for occupational and recreational load carriage. Providing sufficient adaptation time and evaluating the system in a larger number of participants will also be necessary to determine the reproducibility and generalizability of the proposed approach.

Supplementary Materials: The following supporting information can be downloaded at: https://www.mdpi.com/article/10.3390/act15100543/s1, Video S1: XCoM-Based Moving-Mass Control in a Backpack for Modulating Gait Stability During Load Carriage.

Author Contributions: Conceptualization, J.L. and H.S.C.; Data curation, J.L.; Formal analysis, J.L.; Funding acquisition, H.S.C.; Project administration, H.S.C.; Software, J.L.; Supervision, H.S.C.; Visualization, J.L.; Writing—original draft, J.L.; Writing—review and editing, J.L. and H.S.C. All authors have read and agreed to the published version of the manuscript.

Funding: This work was partly supported by the Institute of Information & Communications Technology Planning & Evaluation (IITP) -ICAN (ICT Challenge and Advanced Network of HRD) grant funded by the Korea government (Ministry of Science and ICT) (IITP-2026-RS-2024-00436528, 50%) and by the National Research Foundation of Korea(NRF) grant funded by the Korea government(MSIT) (RS-2024-00452977, 50%).

Institutional Review Board Statement: The study was conducted in accordance with the Declaration of Helsinki, and approved by the Institutional Review Board of Sejong University (protocol code SUIRB-HR-2026-024 and date of approval: 23 June 2026).

Informed Consent Statement: Informed consent was obtained from all subjects involved in the study.

Data Availability Statement: The data presented in this study are available on request from the corresponding author.

Conflicts of Interest: The authors declare no conflicts of interest.

References

1. Liew, B.; Morris, S.; Netto, K. The effect of backpack carriage on the biomechanics of walking: A systematic review and preliminary meta-analysis. *J. Appl. Biomech.* **2016**, *32*, 614–629. [CrossRef] [PubMed]
2. Dempsey, A.M.; Yegian, A.K.; Sibson, B.E.; Lieberman, D.E. The effect of vertical load placement on metabolic rate during loaded walking in humans. *Ergonomics* **2023**, *66*, 849–858. [CrossRef] [PubMed]
3. Park, J.-H.; Stegall, P.; Zhang, H.; Agrawal, S. Walking with aBackpack using load distribution and dynamic load compensation reduces metabolic cost and adaptations to loads. *IEEE Trans. Neural Syst. Rehabil. Eng.* **2017**, *25*, 1419–1430. [CrossRef] [PubMed]
4. Rome, L.C.; Flynn, L.; Yoo, T.D. Rubber bands reduce the cost of carrying loads. *Nature* **2006**, *444*, 1023–1024. [CrossRef] [PubMed]
5. Yang, Z.; Huang, L.; Zeng, Z.; Wang, R.; Hu, R.; Xie, L. Evaluation of the load reduction performance via a suspended backpack with adjustable stiffness. *J. Biomech. Eng.* **2022**, *144*, 051001. [CrossRef] [PubMed]
6. Lin, X.; Yin, S.; Du, H.; Leng, Y.; Fu, C. Biomechanical consequences of walking with the suspended backpacks. *IEEE Trans. Biomed. Eng.* **2024**, *71*, 2001–2011. [CrossRef] [PubMed]
7. Singh, T.; Koh, M. Effects of backpack load position on spatiotemporal parameters and trunk forward lean. *Gait Posture* **2009**, *29*, 49–53. [CrossRef] [PubMed]
8. Qu, X. Effects of cognitive and physical loads on local dynamic stability during gait. *Appl. Ergon.* **2013**, *44*, 455–458. [CrossRef] [PubMed]

9. Xu, D.; Zhou, H.; Quan, W.; Jiang, X.; Liang, M.; Li, S.; Ugbolue, U.C.; Baker, J.S.; Fekete, G.; Ma, X.; et al. A new method proposed for realizing human gait pattern recognition: Inspirations for the application of sports and clinical gait analysis. *Gait Posture* **2024**, *107*, 293–305. [CrossRef] [PubMed]
10. Bauby, C.E.; Kuo, A.D. Active control of lateral balance in human walking. *J. Biomech.* **2000**, *33*, 1433–1440. [CrossRef] [PubMed]
11. O'Connor, S.M.; Kuo, A.D. Direction-dependent control of balance during walking and standing. *J. Neurophysiol.* **2009**, *102*, 1411–1419. [CrossRef] [PubMed]
12. Hof, A.L.; Gazendam, M.G.J.; Sinke, W.E. The condition for dynamic stability. *J. Biomech.* **2005**, *38*, 1–8. [CrossRef] [PubMed]
13. Hof, A.L. The "extrapolated center of mass" concept suggests a simple control of balance in walking. *Hum. Mov. Sci.* **2008**, *27*, 112–125. [CrossRef] [PubMed]
14. Rosker, J.; Markovic, G.; Sarabon, N. Effects of vertical center of mass redistribution on body sway parameters during quiet standing. *Gait Posture* **2011**, *33*, 452–456. [CrossRef] [PubMed]
15. Aerospace Medical Research Laboratory. *Anthropometry and Mass Distribution for Human Analogues, Volume I: Military Male Aviators*; Harry, G., Ed.; AAMRL-TR-88-010; Armstrong Aerospace Medical Research Laboratory: Wright-Patterson Air Force Base, OH, USA, 1988.
16. Malouche, I.; Abbes, A.K.; Bouani, F. Automatic model predictive control implementation in a high-performance microcontroller. In *Proceedings of the 2015 IEEE 12th International Multi-Conference on Systems, Signals & Devices (SSD15) Mahdia, Tunisia, 16–19 March 2015*; IEEE: New York, NY, USA, 2015; pp. 1–6. [CrossRef]
17. Ferreau, H.J.; Kirches, C.; Potschka, A.; Bock, H.G.; Diehl, M. QpOASES: A parametric active-set algorithm for quadratic programming. *Math. Program. Comput.* **2014**, *6*, 327–363. [CrossRef]
18. Palermo, E.; Rossi, S.; Marini, F.; Patanè, F.; Cappa, P. Experimental evaluation of accuracy and repeatability of a novel body-to-sensor calibration procedure for inertial sensor-based gait analysis. *Measurement* **2014**, *52*, 145–155. [CrossRef]
19. Dingwell, J.B.; Cusumano, J.P. Nonlinear time series analysis of normal and pathological human walking. *Chaos An. Interdiscip. J. Nonlinear Sci.* **2000**, *10*, 848–863. [CrossRef] [PubMed]
20. Dingwell, J.B.; Cusumano, J.P.; Cavanagh, P.R.; Sternad, D. Local dynamic stability versus kinematic variability of continuous overground and treadmill walking. *J. Biomech. Eng.* **2001**, *123*, 27–32. [CrossRef] [PubMed]
21. Abram, S.J.; Poggensee, K.L.; Sánchez, N.; Simha, S.N.; Finley, J.M.; Collins, S.H.; Donelan, J.M. General variability leads to specific adaptation toward optimal movement policies. *Curr. Biol.* **2022**, *32*, 2222–2232.e5. [CrossRef] [PubMed]
22. Dingwell, J.B.; Marin, L.C. Kinematic variability and local dynamic stability of upper body motions when walking at different speeds. *J. Biomech.* **2006**, *39*, 444–452. [CrossRef] [PubMed]

Disclaimer/Publisher's Note: The statements, opinions and data contained in all publications are solely those of the individual author(s) and contributor(s) and not of MDPI and/or the editor(s). MDPI and/or the editor(s) disclaim responsibility for any injury to people or property resulting from any ideas, methods, instructions or products referred to in the content.